PII: S0301-5629(01)00495-1

● *Original Contribution*

AXIAL RESOLUTION IN ELASTOGRAPHY

RAFFAELLA RIGHETTI,*[†] JONATHAN OPHIR*[†] and PERIKLIS KTONAS[†]
*The University of Texas Medical School, Department of Radiology, Ultrasonics Laboratory, 6431 Fannin St.,
Houston, TX, USA; and [†]University of Houston, Electrical and Computer Engineering Department,
4800 Calhoun Rd., Houston, TX, USA

Abstract—The limits and trade-offs of the axial resolution in elastography were investigated using a controlled simulation study. The axial resolution in elastography was estimated as the distance between the full widths at half-maximum of the strain profiles of two equally stiff lesions embedded in a softer homogeneous background. The results show that the upper bound of the axial resolution in elastography is controlled by the physical wave parameters of the ultrasound (US) system used to acquire the data (transducer center frequency and bandwidth). However, an inappropriate choice of the parameters used to process the US data (cross-correlation window length and shift between consecutive windows) may compromise the best resolution attainable. The measured elastographic axial resolution was found to be on the order of the ultrasonic wavelength. (E-mail: Jonathan.Ophir@uth.tmc.edu) © 2002 World Federation for Ultrasound in Medicine & Biology.

Key Words: Ultrasound, Elastography, Axial resolution, Wavelength, Bandwidth, Cross-correlation.

INTRODUCTION

Resolution is one of the primary parameters utilized to characterize the performance of an imaging system. Generally, there is no unique definition of resolution, and its measurement may vary according to the definition that is used. One of the fields in which resolution has been explicitly defined is optics (Houston 1934; Rayleigh 1879). The resolution of an optical system is usually regarded as a measure of the ability of the system to distinguish between two closely spaced point sources, and it is, therefore, related to the point spread function of the system (Gaskill 1978). In optics, there are several criteria for specifying resolution, and the most common one is the Rayleigh criterion (Rayleigh 1879). In sonography, the axial resolution is a measure of the ability of an instrument to resolve two reflecting boundaries that are closely spaced in the axial direction (Christensen 1988). A simplified theoretical expression for the sonographic axial resolution (AR) for a spherical radiator at the focus is given by (Christensen 1988):

$$AR = (Q \times \lambda)/4, \quad (1)$$

where Q is the quality factor of the transducer and λ is the wavelength. Equation (1) shows that an improved sonographic axial resolution is a result of a higher transducer fractional band width ($Q = 1$/fractional bandwidth), at a given wavelength λ, and/or an increase in the center frequency (or a decrease in the wavelength λ), for a constant Q.

Elastography is a new imaging modality that is capable of mapping the local strains that are experienced by the tissue due to the application of a small compression (displacement) (Ophir et al. 1991, 1999). Internal axial tissue strains are estimated from the analysis of pre- and postcompression digitized radiofrequency (RF) echo signals, using standard diagnostic ultrasound (US) equipment. Congruent echo lines are subdivided into partially overlapped small temporal windows that are compared pairwise using cross-correlation techniques. The local tissue strains (gradients of the estimated tissue displacement field) are displayed as an image known as an elastogram. The performance of elastography is usually described in terms of elastographic signal-to-noise ratio (SNRe), elastographic contrast-to-noise ratio (CNRe), elastographic dynamic range (DRe), sensitivity and resolution. The performance of elastography depends mainly on three groups of parameters (Varghese and Ophir 1996, 1997). The first group is related to the physical parameters of the US system used to acquire the

Address correspondence to: Dr. Jonathan Ophir, The University of Texas Medical School, Department of Radiology, Ultrasonics Laboratory, 6431 Fannin St., Houston, TX 77030 USA. E-mail: Jonathan.Ophir@uth.tmc.edu

data. These parameters are usually referred to as the ultrasonic parameters, the most important of which are the transducer center frequency f_0, the bandwidth B, the sonographic signal-to-noise ratio (SNRs) and the beamwidth. The second group is related to the parameters that are used to process the digital signals to create the image. These parameters are usually referred to as the digital signal-processing (DSP) parameters and, among them, the most important ones are the length Z (in mm) of the cross-correlation window used to segment the RF data, and the translation step (shift) ΔZ between two consecutive cross-correlation windows (Ophir et al. 1999). A third group of parameters that affect elastographic performance includes the acoustic and mechanical properties of tissue (Kallel et al. 2001; Ophir et al. 1999).

Extensive studies have been done to characterize the SNRe, CNRe, DRe and sensitivity of elastograms (Konofagou et al. 1997; Ponnekanti et al. 1995; Varghese and Ophir 1997). In contrast, very little quantitative information is available on the resolution in elastography. Although the term "elastographic resolution" has been widely used recently (Alam et al. 2000; Cohn et al. 1997; Cook et al. 2000; Schmitt et al. 1999; Varghese et al. 1998), a formal theoretical definition does not exist in the literature. In the past, the elastographic axial resolution was considered to be equivalent to the cross-correlation window length (Cespedes 1993; Varghese et al. 1998). Only recently, Alam et al. (2000) showed that the resolution is a function of both the window shift ΔZ and the window length Z, with ΔZ being more important than Z. This was shown using a simulation experiment and assuming a given US system; hence, keeping all the ultrasonic parameters constant. Alam and colleagues estimated the elastographic axial resolution using a 1-D wedge phantom model with low elastic contrast compared to the background, and utilizing the gradient strain estimator method with global uniform stretching (Varghese and Ophir 1997). They defined the resolution as the smallest width of the wedge for which the estimated strain profile corresponding to each A-line dropped below the midpoint between the maximum and minimum strains. According to this definition, they found an elastographic resolution ranging between 0.125 mm and 2 mm (*i.e.,* on the order of the sonographic resolution for the simulated US system). Their curve of the resolution as a function of the shift ΔZ, for any given Z, shows that the resolution changes linearly with the window shift. However, interestingly, for values of ΔZ below a certain empirical threshold, the curve shows a "knee" and a plateau indicating that, below this threshold, the resolution is insensitive to the DSP parameters used to process the data and cannot be further improved by changing them.

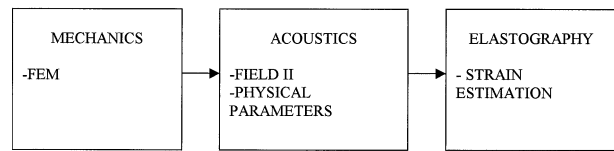In general, the knowledge of the limits and trade-

Fig. 1. The block diagram (highly simplified) of the procedure followed to estimate the axial resolution in elastography. The entire procedure consists of three steps. A finite-element-simulation phantom containing two equally stiff lesions with Gaussian modulus profile is generated ("mechanics" block). The acoustic intensity field inside the phantom before and after compression for a given simulated US system is simulated ("acoustics" block). The pre- and postcompression RF A-lines are processed using cross-correlation techniques to estimate the displacement field and the axial strain distribution in the phantom ("elastography" block).

offs for the resolution of an imaging system is crucial for correct interpretation of the images and, consequently, for evaluation of feasible applications of the imaging modality at any scale. This is especially important at the microscopic scale, where the objective is to optimize the imaging of small structures and, in general, to obtain information not available from the corresponding conventional macroscale applications. In the last few years, there has been an increasing interest in the so-called "microscopic elastography" (Fortin et al. 2000; Schmitt et al. 1999), also referred to as "elasticity microscopy" (Cohn et al. 1997). Microscopic elastography refers to the application of basic elastographic principles while using high-frequency US systems to acquire the data, and it may have significant potential for applications in dermatology, ophthalmology and pathology.

In this study, we investigated the parameters that fundamentally limit the axial resolution in elastography. We analyzed the effects of the ultrasonic parameters, the DSP parameters, and the lesion/background elastic contrast on the attainable resolution, using a 2-D simulation study. Our hypothesis is that the elastographic axial resolution is ultimately limited by the physical parameters of the US system used to acquire the data. However, we also hypothesize that an inappropriate choice of the DSP parameters used to process the ultrasonic data may corrupt the achievable resolution. More details on this study may be found in Righetti (2001).

METHODS

We used simulated finite-element phantoms, generated with a commercial software package (ALGOR, Inc., Pittsburgh, PA). The entire simulation tool consisted of three successive steps, as shown in the block diagram of Fig. 1. First (Fig. 1, "mechanics" block), we generated finite-element-simulation phantoms, consisting of homo-

geneous tissues containing two stiff circular lesions of equal lesion/background elastic modulus contrast. Each simulated phantom had dimensions of 5 mm × 5 mm, was fixed at the bottom, free on the sides and compressed from the top. We assumed slip boundary conditions and a 2-D plane-strain state model. The two stiff lesions were axisymmetrically placed in the center of the phantom. To avoid abrupt changes in the elastic modulus of the phantom, a 2-D approximately Gaussian-distributed elastic modulus was assigned to each lesion. The two Gaussian lesions were truncated at two SD, and the effective diameter of each lesion was then normalized to 1 mm. The axial distance between the two Gaussian distributions at their half-maximum profile was varied for each finite-element model. To investigate the effect of the lesion/background elastic contrast on the elastographic axial resolution, we performed the entire study for both high and low lesion/background elastic contrast values. In the high-contrast case, the center of the lesion was approximately 10 times stiffer than the background and, in the low-contrast case, the center of the lesion was approximately 2 times stiffer than the background. The outputs of the first block of the simulation process (Fig. 1, "mechanics" block) are the elastic modulus distribution inside the phantom and the axial displacement that each node of the finite-element model experiences after the application of a uniaxial compression.

The second step (Fig. 1, "acoustics" block) involved simulation of the acoustic pressure field inside the phantoms before and after compression. We assumed that each phantom consisted of 2.5×10^5 randomly positioned scatterers, with Gaussian-distributed backscatter cross-sections. The acoustic pressure field associated with each US system model was simulated using FIELD_II, an acoustic field simulation program (http://www.it.dtu.dk/~jai/field/). Various transducer models (different center frequencies, bandwidths and beamwidths) were simulated. All the transducers were modeled as single-element focused circular transducers, with a 3-mm radius aperture and center frequencies ranging from 5 MHz to 100 MHz. The sampling frequency was fixed at 20 times the center frequency of the transducer. To investigate the effect of the bandwidth of the transducer and, hence, its quality factor on the elastographic axial resolution, we performed the entire study for three different values of the fractional bandwidth (80%, 55% and 35%). The bandwidth was defined as the frequency width of the transducer power spectral density at −6-dB. The beamwidth was maintained constant at the focus (0.5 mm) for all cases (*i.e.,* the focal length of each transducer was adjusted to have a beamwidth at the focus of approximately 0.5 mm at all frequencies). To have a qualitative idea of the effect of the beamwidth on the measured axial resolution at one particular frequency (50

MHz), we estimated the resolution also for a beamwidth of approximately 0.2 mm. All the resolution estimations were obtained assuming that the two lesions were positioned at the focus of the transducer, and neglecting the effect of attenuation. Each phantom was compressed axially by 1% of its entire height, and the RF images of the phantom before and after tissue compression were computed. To obtain each RF image, the transducer was moved across the sample in steps of 0.05 mm, for a total of 50 A-lines. Therefore, the dimensions of each RF image (and corresponding elastogram) were 5 mm (depth) by 2.5 mm (width), with the lesions positioned at the center of the image. Initially, we assumed that no lateral motion had occurred. Thereafter, we also investigated the effect of the lateral motion of the scatterers on the results. No noise was added to the signals. The outputs of the second block of the simulation process (Fig. 1, "acoustics" block) are the precompression RF A-lines and the postcompression RF A-lines.

Finally (Fig. 1, "elastography" block), we estimated the displacement field and the axial strain distribution in the phantom from the simulated pre- and postcompression RF data, using cross-correlation techniques. The elastograms were processed using the gradient strain estimator with global stretching (Varghese and Ophir 1996). To determine the best DSP parameters to process the simulated RF signals, elastograms were generated for different values of the cross-correlation window length Z. The values of the cross-correlation window length ranged between 0.01 mm and 2 mm (in steps of 0.01 mm). The shift ΔZ between windows was fixed at 5% of Z (which corresponds to a 95% overlap between consecutive windows). Median filters (1-D) were used to reduce the noise spikes in the displacement images. Preliminary simulations were used to determine a value for the appropriate median filter kernel for this study. A generally appropriate kernel size was found to be $\lambda/2$, where λ is the central acoustic wavelength (Righetti 2001).

The elastographic axial resolution was estimated as the distance between the full widths at half-maximum of the strain profiles corresponding to the two lesions, measured from the simulated strain images. According to the model used in this work, the two lesions are resolvable if the estimated strain profile across the two lesions rises above the −6-dB difference between the average strain inside the lesions and the average strain in a homogeneous region of the tissue. An example of the procedure to estimate the resolution is illustrated in Fig. 2. The first image (a) is the "ideal" strain image obtained under the mechanical compression conditions and assuming a plane-strain state problem, without the involvement of any acoustical parameters. Note the presence of mechanical strain concentrations around the lesions, which is characteristic for the strain distribution of the mechanical
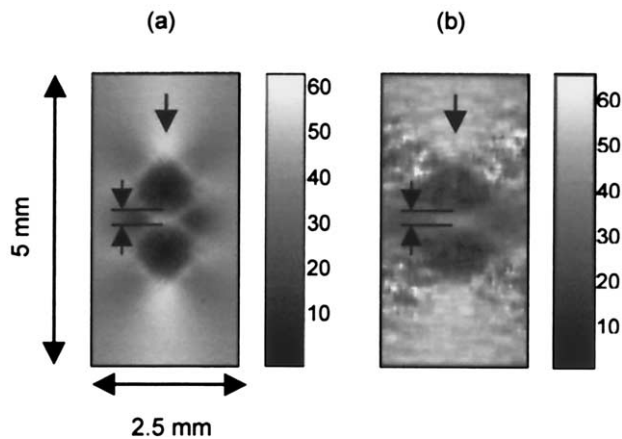
Fig. 2. Illustration of the procedure used to estimate the axial resolution in elastography. (a) Ideal strain image, obtained under mechanical compression conditions and plane-strain state boundary conditions. (b) Corresponding actual strain image or axial strain elastogram estimated simulating a 50-MHz US system. Each shown image is 5 mm (depth) by 2.5 mm (width). In both images, the axial distance between the axial strain profiles of the two elastically Gaussian lesions at half-maximum is pointed out (0.3 mm).
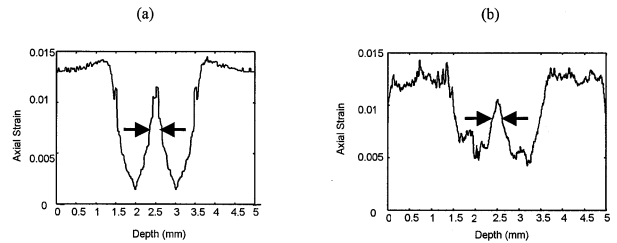

Fig. 3. (a) Strain profile from the ideal strain image of Fig. 2a taken axially across the center of the lesions. (b) Strain profile from the elastogram of Fig. 2b taken axially across the center of the lesions. The arrows point out the −6-dB threshold, which is determined as the midpoint between the average strain outside the lesions and the average strain inside the lesions. The actual resolution is computed as the width of the peak at the −6-dB level from the estimated elastogram (Figs. 2b and 3b). Note the loss of CNRe in the elastogram when compared to the ideal strain image. This is probably due to the use of a small value of cross-correlation window length to process the elastogram of Fig 2b. Despite the loss of contrast, the measurements of the width of the peaks at the threshold level are approximately the same for both (a) and (b), and close to the real known distance within an error of 20%. Note the presence of noise also in the ideal strain profile, which is probably due to the limited resolution of the finite-element model mesh. The CNR of the ideal strain images was found to be sufficiently high so that the influence of this noise on the resulting elastograms could be practically neglected.

model geometry used. The second image (b) represents the estimated strain image (or axial strain elastogram) that is obtained from high-frequency ultrasonic RF data generated using a 50-MHz center frequency transducer, with the limitations of the ultrasonic and signal-processing parameters. In both images, the axial distance between the strain profiles of the two lesions at their half-maximum is indicated. Then, the actual axial resolution is computed as the width of the peak at the −6-dB threshold for the smallest resolvable distance. Figure 3 shows the axial profiles of the "ideal" strain (Fig. 3a) and the estimated strain (Fig. 3b), taken from the center of the corresponding "ideal" strain image (Fig. 2a) and the corresponding elastogram (Fig. 2b). The resolution relates to the minimum possible distance indicated by the two arrows in Fig. 3b.

The entire procedure for a given ultrasonic frequency may be summarized as follows. First, a finite-element model (FEM) corresponding to a known distance between the lesions was generated. Second, the acoustic pressure field associated with a given transducer was computed, for 24 realizations of the random distributions of scatterers. Third, a series of elastograms was computed for different values of the cross-correlation window length Z and for each of the 24 realizations (the shift ΔZ was maintained as a fixed percentage of Z). Then, we analyzed the resolution measurements obtained for each realization at the various values of Z and determined if a value of Z existed for which all 24 realizations showed measurements greater than the known real dis-

tance, within an error of less than 20%. If this were the case, we then concluded that this particular distance was resolvable at the given frequency and at the given value of Z. If more than one value of Z permitted resolving a particular distance, we chose the value of Z for which the average of the 24 measurements was closest to the real distance. Thereafter, we considered a smaller distance between the two lesions and, after repeating the entire procedure, we determined if this smaller distance was resolvable. For a given ultrasonic frequency, we stopped the process when we found a distance that was no longer resolvable for any value of Z. To further determine the optimal value of the cross-correlation window length, we considered a narrow range of values around the value of Z for which we could resolve the given distance (with the smallest error) and, for each realization, we evaluated the best Z inside that range. The final optimal value of Z was determined as the average over the 24 best values. At that point, we computed the resolution for that given frequency as the average over the 24 estimations of the smallest resolvable distance, using that optimal cross-correlation window length. We then moved to the next ultrasonic frequency.

We also computed the values of the axial resolution using the same value of Z for the entire range of frequencies. For each frequency, we considered a total of 16 realizations of the random distributions of scatterers. We

considered three cases: $Z = 0.4$ mm, $Z = 0.2$ mm, and $Z = 0.12$ mm. For each of the three cases, we also evaluated an error criterion (absolute difference between the mean of 16 measurements of the axial resolution computed with Z constant and the mean of 16 measurements of the axial resolution computed with Z normalized to the wavelength.

To investigate the effect of the cross-correlation window length Z and the shift between windows ΔZ on the attainable axial resolution, we measured the resolution for different values of Z and ΔZ, assuming fixed ultrasonic parameters. To analyze the effect of the cross-correlation window length Z, we considered two cases. In the first case, the ultrasonic frequency was fixed at 20 MHz (bandwidth at 80% of the center frequency, beamwidth at 0.5 mm), and Z ranged between 0.1 mm and 0.5 mm. In the second case, the ultrasonic frequency was fixed at 50 MHz (bandwidth at 80% of the center frequency, beamwidth at 0.5 mm), and Z ranged between 0.04 mm and 0.5 mm. In both cases, the shift ΔZ was a fixed percentage of Z (5%). To analyze the effect of ΔZ, we computed the axial resolution for different values of the shift, maintaining Z constant (two cases, $Z = 0.2$ and $Z = 0.3$ mm) and the ultrasonic parameters constant (20 MHz, 80% fractional bandwidth, 0.5 mm beamwidth).

We estimated the resolution for both high and low lesion/background elastic contrast. To investigate the effect of the elastic contrast alone on the attainable resolution, we used the same values of the ultrasonic and DSP parameters for both the high and low-contrast cases. For the high-contrast case, the resolution was estimated as the average over 16 realizations. To reduce the noise and accurately estimate the axial resolution for the low-contrast case, we averaged a higher number of realizations for a given frequency. For the low-contrast case, the resolution was estimated as the average over 16 realizations, each of them being the average over 5 realizations.

Finally, to investigate the effect of scatterer motion on the elastographic resolution, we simulated elevationally confined phantoms, eliminating the assumption of no lateral motion of scatterers, and repeated the entire resolution measurements for 24 different realizations of the random distributions of scatterers.

RESULTS

The results of this study are classified under three main categories. In the first category, we analyze the limitations of the axial resolution in elastography due to the ultrasonic parameters. In the second category, we investigate how the choice of the digital signal-processing parameters influences the obtainable resolution. Finally, in the third category, we compare the results of the
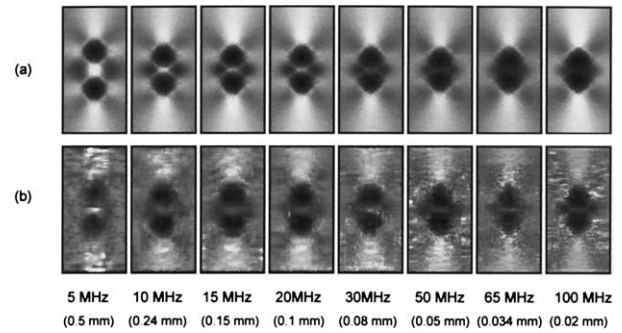

Fig. 4. (a) Set of ideal strain images and (b) corresponding elastograms. The elastograms in (b) were obtained by simulating transducers of center frequencies specified at the bottom of the elastograms (bandwidth: 0.8 f_0; beamwidth approximately 0.5 mm for each case except for 5 MHz where the beamwidth was approximately 1 mm). For each frequency, the corresponding elastogram refers to the mechanical model with the two lesions being spaced at the estimated resolution at that particular frequency. Each elastogram was obtained by processing the RF data using the gradient strain estimator with global stretching and values of Z reported in Fig. 6 for each frequency ($\Delta Z = 0.05 Z$). A 1-D median filter (kernel size = $\lambda/2$) was applied to each strain image to reduce the noise spikes. For the purpose of illustration, the elastograms of (b) were obtained by averaging five different realizations of the same mechanical model (different random distribution of the scatterers inside the phantom). The corresponding known distance between the lesions (from the modulus images) is specified at the bottom of the elastograms, at any given frequency.

elastographic axial resolution obtained for two cases of lesion/background elastic contrast (high and low).

Effect of ultrasonic parameters

Figure 4 shows a set of ideal strain images (Fig. 4a) and matching elastograms (Fig. 4b). The elastograms are the strain images estimated by simulating transducers of center frequencies that are specified at the bottom of the elastograms. For each frequency, the corresponding elastogram refers to the mechanical model with the two lesions being spaced at the minimum resolvable distance at that particular frequency. The corresponding known distance between the lesions is specified at the bottom of the elastograms, at any given frequency. For the purpose of illustration, the elastograms of Fig. 4b were obtained by averaging five elastograms, each of them estimated from a phantom possessing constant mechanical properties, but with different random distributions of the scatterers. Figure 5 shows the values of the elastographic axial resolution as a function of the transducer center frequency (average over 24 realizations, each of them obtained from raw data), as measured from the elastograms. The solid curve refers to the resolution measurements obtained when assuming no lateral motion of
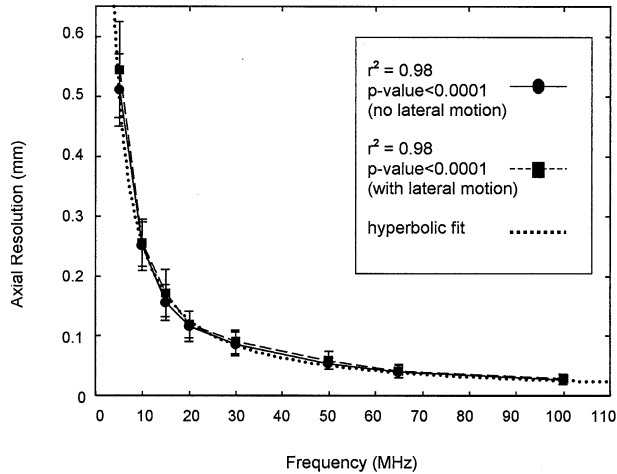
Fig. 5. Estimated elastographic axial resolution (mm) as a function of the transducer center frequency (MHz). (—●—) resolution measurements obtained when assuming no lateral motion of scatterers; (—■—) case in which the scatterers were free to move both in the axial and in the lateral direction after the compression of the phantom; (· · · ·) hyperbola fitted to the measurement points obtained when assuming no lateral motion of scatterers. For the purpose of illustration, the hyperbola fitted to the measurement points obtained in the case of lateral motion of scatterers is not shown. The error bars represent the SD over 24 estimations. The values of resolution were obtained by processing the raw data using the values of cross-correlation window length shown in Fig. 6 at any given ultrasonic frequency. A 1-D median filter (kernel size = $\lambda/2$) was applied to each elastogram. Observe the high coefficient of determination (approximately 0.98) between the elastographic resolution measurements and a hyperbola fitted to these measurements, for both data sets. These high coefficients suggest proportionality between the elastographic axial resolution and the ultrasonic wavelength, with the constant of proportionality being approximately equal to 1.5, for both cases.
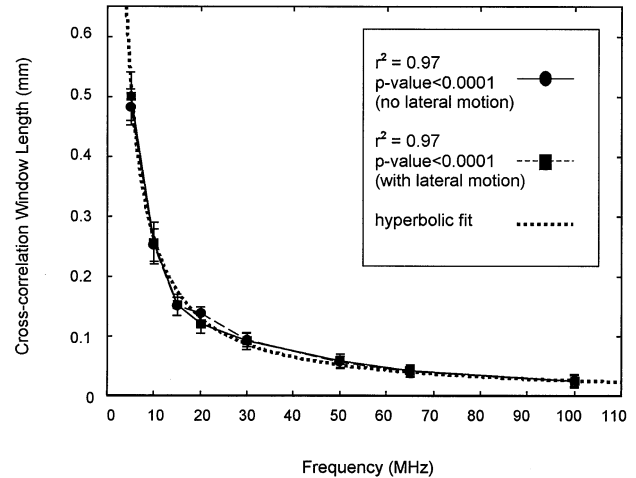
Fig. 6. Optimal cross-correlation window lengths (mm) as a function of the transducer center frequency (MHz). (—●—) resolution measurements obtained when assuming no lateral motion of scatterers; (—■—) case in which the scatterers were free to move both in the axial and in the lateral direction after the compression of the phantom; (· · · ·) hyperbola fitted to the measurement points obtained when assuming no lateral motion of scatterers. For the purpose of illustration, the hyperbola fitted to the measurement points obtained in the case of lateral motion of scatterers is not shown. The error bars represent the SD over 24 estimations. These optimal cross-correlation window lengths were determined as the values of Z for which the smallest distance was resolvable at any given frequency. The high determination coefficients between measurement points and hyperbolas fitted to the data suggest proportionality between the optimal window length and the ultrasonic wavelength, with the constant of proportionality being approximately equal to 1.6, for both cases.

scatterers, and the dashed curve refers to the case in which the scatterers were free to move both in the axial and in the lateral direction after the compression of the phantom. The error bars represent the SD over 24 estimations. For both sets of measurements, we computed the coefficient of determination between the measurement points related to one of the data sets and a hyperbola fitted to the same measurement points. For the purpose of illustration, only one of the two hyperbolas (the one fitted to the measurements obtained under the assumption of no lateral motion) is shown in Fig. 5 (dotted line). The high coefficients of determination ($r^2 = 0.98$) between the measurement points and the two hyperbolas fitted to the two measurement sets suggest an inverse proportionality between the elastographic axial resolution and the ultrasonic frequency. Additional statistical analyses of these measurements were done. We constructed the 95% confidence intervals (CI) for the true means of the axial resolution for each frequency, and

we computed the coefficient of determination between the upper and the lower bounds of the CI and the hyperbola. From this analysis, we can infer that there is no statistically significant difference between the true means of the axial resolution (within the 95% CI) and the fitted hyperbola, which corroborates the hypothesis that the elastographic axial resolution is inversely proportional to the ultrasonic frequency.

In performing the resolution measurements, we observed that the value of the cross-correlation window length Z needed to be properly adjusted at any given frequency to optimize the axial resolution. The cross-correlation window lengths, for which we obtained the results of Fig. 5, are plotted with respect to frequency in Fig. 6, both in the case of no lateral motion (solid curve) and in the case of possible lateral motion of scatterers (dashed curve). In both cases, we computed the coefficient of determination between the measurement points related to one of the data sets and a hyperbola fitted to the same measurement points. For the purpose of illustration, only one of the two hyperbolas (the one fitted to the
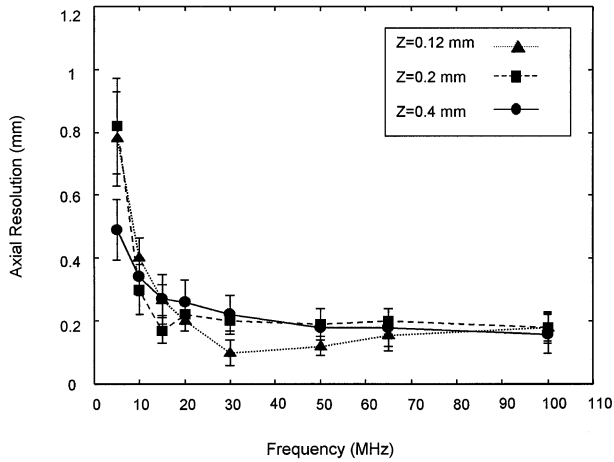
Fig. 7. Elastographic axial resolution (mm) estimated by using a fixed value of cross-correlation window length for the entire range of ultrasonic frequencies. Three cases are reported (Z = 0.4 mm, Z = 0.2 mm and Z = 0.12 mm). The error bars represent the SD over 16 different realizations. Observe that each value of Z gives better results for a certain frequency range.

Fig. 8. Error (absolute difference) between the mean of 16 measurements of the axial resolution computed with Z constant and the mean of 16 measurements of the axial resolution computed with Z normalized to the wavelength. The reported errors refer to the three cases shown in Fig. 7.

measurements obtained under the assumption of no lateral motion) is shown in Fig. 6 (dotted line). The high coefficients of determination (r^2 = 0.97) between the measurement points and the two hyperbolas drawn through the two measurement sets suggest an inverse proportionality between the cross-correlation window lengths and the ultrasonic frequency. As for the axial resolution case, similar statistical analyses were carried out for the cross-correlation window length Z. From this analysis, we can infer that there is no statistically significant difference between the true means of the optimal value of Z (within the 95% CI) and the fitted hyperbola, which corroborates the hypothesis that the optimal cross-correlation window length is inversely proportional to the ultrasonic frequency.

Additional statistical analysis for both resolution and optimal Z data points showed that no statistically significant difference exists between the set of measurements obtained under the assumption of no lateral motion of scatterers and the set obtained when accounting for scatterer lateral motion. Based on the above statistical results, we proceeded in our measurements by utilizing simulations under the assumption that no lateral motion occurred. The results presented in the following paragraphs are based on this particular assumption.

Figure 7 shows the measurements of the axial resolution obtained using a constant value of the cross-correlation window length for all frequencies. Figure 8 shows the error (absolute difference) between the mean of 16 measurements of the axial resolution computed with Z constant and the mean of 16 measurements of the
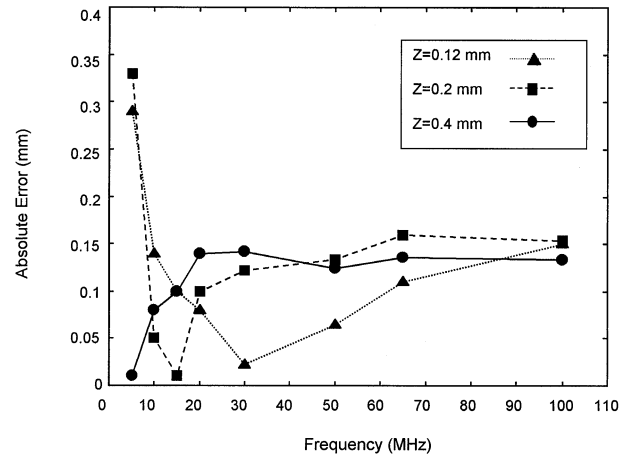
axial resolution computed with Z normalized to the wavelength. Observe from Fig. 7 and Fig. 8 that each value of Z gives better results for a certain frequency range, but that, outside this range, the resolution is seriously compromised. The largest window works better at low frequencies (5 MHz), where using smaller windows introduces high error in the estimation. For frequencies between 10 MHz and 15 MHz, the intermediate value of Z produces the best resolution. Above 20 MHz until 50 MHz, the smallest window performs better, and for very high frequencies (above 50 MHz), all three values of Z produce high error in the estimation. For all cases (Z = 0.4 mm, Z = 0.2 mm, and Z = 0.12 mm), we compared the measurements corresponding to each pair of adjacent frequencies. For the case of Z = 0.4 mm, there are no statistically significant differences among the true means of the measurements at frequencies higher than 10 MHz (at a 95% confidence level). The same type of analysis was applied for the results obtained at Z = 0.12 mm, where the measurements corresponding to 30 MHz were found to be statistically different and better than those measured at 20 MHz and/or at 50 MHz. The estimations of the resolution at 20, 65 and 100 MHz show no statistically significant differences among the means of the measurements obtained with the three different values of Z (*i.e.*, the resolution is almost the same in all cases). However, for the other frequencies, there is a significant improvement if we use one of the specific windows. This is particularly evident for the 5-MHz case and the 30-MHz case. The above findings corroborate the hypothesis of the existence of an optimal range of Z for any given ultrasonic frequency.

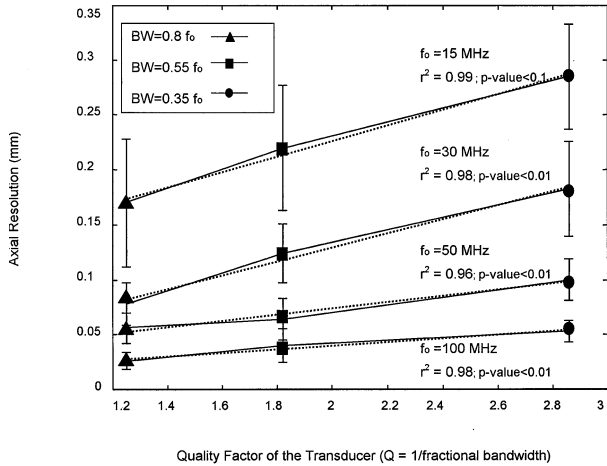Figures 9 and 10 show measurements of the reso-

Fig. 9. Estimated elastographic axial resolution (mm) as a function of the quality factor of the transducer for four cases of ultrasonic frequency (15, 30, 50 and 100 MHz). The error bars represent the SD over 16 different realizations. Observe that, at a given frequency, the improvement of the axial resolution is proportional to the increase of the fractional bandwidth.

Fig. 11. (a) Ideal strain image of the mechanical model of two lesions separated by 0.04 mm. (b) Corresponding elastogram obtained simulating a 50-MHz transducer with 80% fractional bandwidth and 0.2 mm beamwidth. (c) Corresponding elastogram obtained simulating a 50-MHz transducer with 80% fractional bandwidth and 0.5 mm beamwidth. The two elastograms were obtained by averaging five different realizations and using the same digital signal-processing parameters ($Z = 0.064$ mm, $\Delta Z = 0.05\ Z$, median filter kernel size $= \lambda/2$).

lution and the corresponding cross-correlation window lengths, respectively, as a function of the quality factor of the transducer (*i.e.,* inverse fractional bandwidth) at four given frequencies (15, 30, 50 and 100 MHz). In both figures, a line fitted to the measurement points and the corresponding *p*-value and coefficient of determination (between the data points and the line) are shown for each

set of measurements. The high coefficient of determination shows a statistically significant presence of a linear trend. Additional statistical analyses showed that there exists a statistically significant difference (*p*-values $<$ 0.01) between the means of the resolution at a 35% fractional bandwidth and those at a 80% fractional bandwidth for each ultrasonic frequency greater than 15 MHz. For lower frequencies, no firm conclusion could be drawn due to the larger error bars in the measurements. The above analysis holds also for the optimal values of the cross-correlation window length.

As a result of the above, both the elastographic axial resolution and the optimal cross-correlation window length are proportional to the ultrasonic wavelength for a fixed fractional bandwidth and inversely proportional to the fractional bandwidth for a fixed ultrasonic frequency.

Figure 11a shows the ideal strain image of the mechanical model of two lesions spaced 0.04-mm apart. Figures 11b and c show two corresponding elastograms, obtained by simulating a transducer having the same center frequency (50 MHz) but different beamwidth (0.2 mm and 0.5 mm, respectively). Figure 12 shows the axial profiles of the strains taken from the centers of Fig. 11b (dotted line) and Fig. 11c (solid line). From the elastograms of Figs. 11b and c, and from the corresponding axial strain profiles (Fig. 12), there appears to be a slight improvement when the beamwidth is decreased. However, at this time, no firm conclusion regarding any connection between the elastographic axial resolution and the ultrasonic beamwidth can be drawn because we have considered only one case.
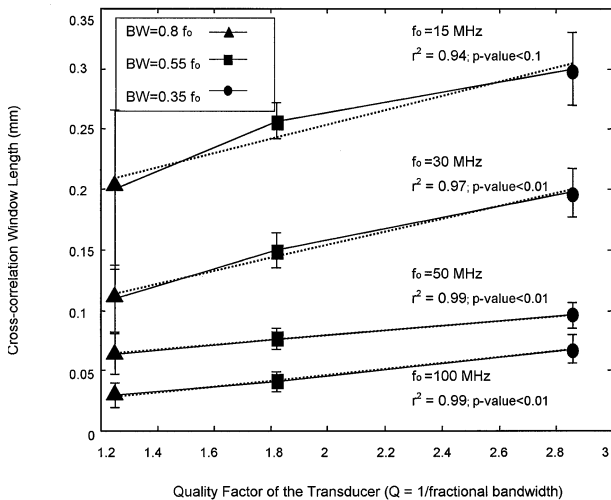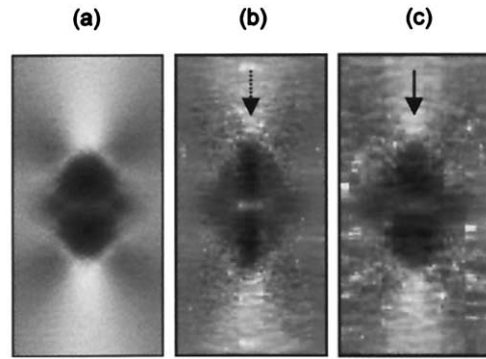

Fig. 10. Optimal cross-correlation window lengths (mm) as a function of the quality factor of the transducer for four cases of ultrasonic frequency (15, 30, 50 and 100 MHz). The error bars represent the SD over 16 different realizations. Observe that, at a given frequency, the optimal cross-correlation window lengths are inversely proportional to the fractional bandwidth.
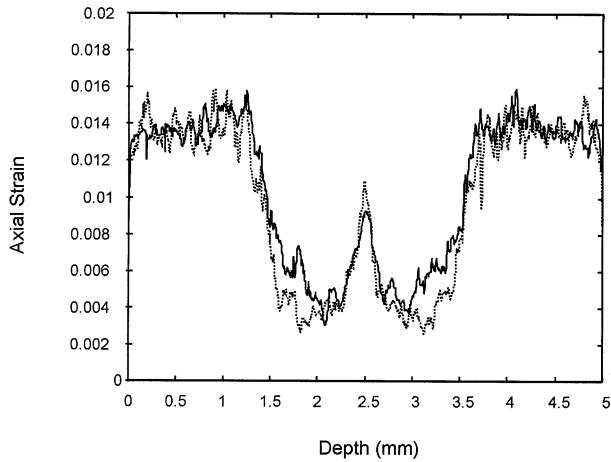
Fig. 12. Axial profiles of the strains taken from the center of Figs. 11b (.....) and Fig. 11c (—). Observe the slight improvement in the separability of the lesions when decreasing the beamwidth.

Fig. 14. A set of elastograms obtained for the US system at 50 MHz, when varying the cross-correlation window length *Z*. Observe the increase of the smoothness in the images when increasing *Z* at the expense of the measured axial resolution.

Effect of DSP parameters

The results concerning the effect of *Z* on resolution are shown in Fig. 13. Observe that, starting from relatively high values of the cross-correlation window length, the resolution tends to improve with decreasing *Z* until a certain value is reached. Afterwards, if we de-

crease *Z* further, the resolution does not improve. Statistical analyses corroborated this result (95% confidence level). Figure 14 shows the elastogram set corresponding to the measurements plotted in Fig. 13 for a center frequency of 50 MHz. Observe that, for larger values of *Z*, the images are smoother and, consequently, the SNRe tends to increase at the expense of the measured axial resolution.

The results concerning the effect of Δ*Z* on resolution are shown in Fig. 15. Observe that the resolution tends to improve with decreasing Δ*Z*. However, statistical analyses showed that, beyond a certain value of Δ*Z*, there is no significant difference (95% confidence level) in the estimated values of the resolution and, therefore, the resolution does not improve further with decreasing Δ*Z*.
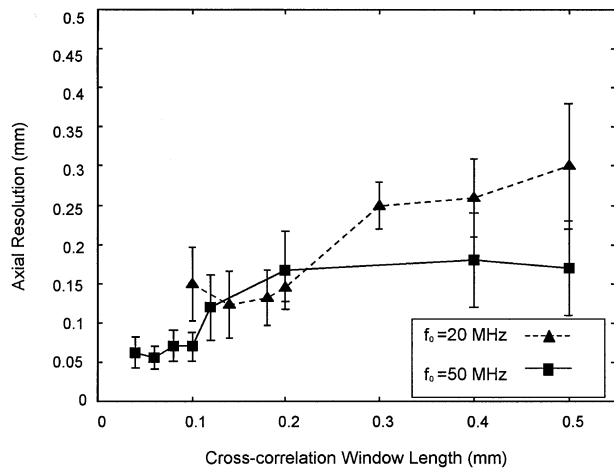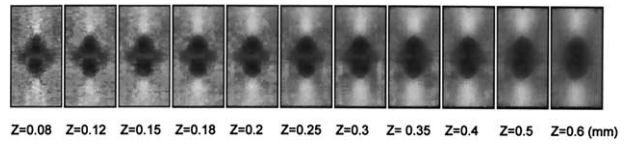

Fig. 13. Estimated elastographic axial resolution (mm) as a function of the cross-correlation window length (mm) for a given US system. Two cases are reported. In one case, we simulated an US system having a 20-MHz transducer, 80% fractional bandwidth and 0.5 mm beamwidth. In the other case, we simulated an US system having a 50-MHz transducer, 80% fractional bandwidth and 0.5 mm beamwidth. The error bars represent the SD over 16 different realizations. Observe the presence of an optimal range of values of *Z* for both cases (around 0.05 mm for the 50-MHz system and 0.15 mm for the 20-MHz system).
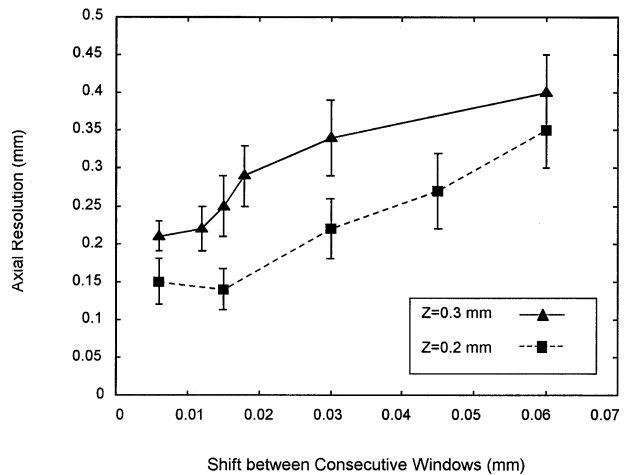

Fig. 15. Estimated elastographic axial resolution (mm) as a function of the shift between consecutive cross-correlation windows (mm), for a given ultrasound system (20 MHz, 80% fractional bandwidth, 0.5 mm beamwidth). The cross-correlation window length was maintained fixed. Two cases are reported (*Z* = 0.2 mm and *Z* = 0.3 mm). The error bars represent the SD over 16 different realizations. Observe that, below a certain value of the shift Δ*Z*, the resolution does not improve further.
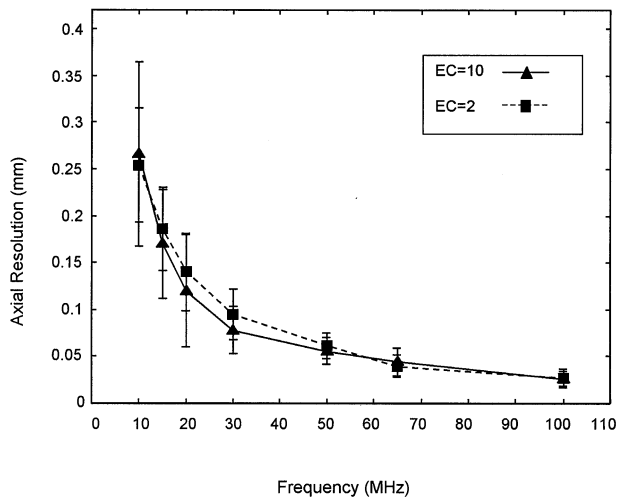
Fig. 16. Estimated elastographic axial resolution (mm) as a function of the transducer center frequency (MHz) for two cases of lesion/background elastic contrast (low: 2, and high: 10). For both cases, the same values of DSP parameters were used to process the data. The error bars for the curve that refers to the high-contrast case represent the SD over 16 different realizations. The error bars for the curve that refers to the low-contrast case represent the SD over 16 different realizations, each of them being an average over five realizations. Observe that, generally, no significant difference exists between the measurements obtained for the low-contrast and the high-contrast case.

Effect of elastic contrast

Figure 16 shows the axial resolution measurements obtained for two different lesion/background elastic contrast levels. Statistical analysis showed that, generally, the resolution does not depend on the elastic contrast (95% confidence level).

DISCUSSION

All previous literature on the elastographic resolution was aimed at understanding how the digital signal-processing parameters affect the axial resolution for a given US system. No previous systematic and statistical studies exist that show how the resolution in elastography is related to the physical parameters of the US system used to acquire the data. In this paper, the limitations and the trade-offs of the axial resolution in elastography were investigated. Because many parameters influence the performance of elastography, it is difficult to evaluate the effect of each of them on the resolution simultaneously. Therefore, our approach consisted in trying to reduce the dimensionality of the problem to a single independent parameter, the central wavelength λ (or the center frequency f_0). The choice of the wavelength as the independent parameter and the description

of the resolution as a function of it originated from two considerations. First, the resolution of the US imaging modality is limited by the wavelength for a fixed fractional bandwidth; therefore, it was postulated that the resolution of elastography, which relies on ultrasonic signals, would be limited by the wavelength for a fixed fractional bandwidth as well. Second, we evaluated the possibility of relating all the remaining elastographic parameters (bandwidth, Z, ΔZ) to the wavelength. Initially, we considered the bandwidth as a fixed percentage of the center frequency. However, because the resolution of the US imaging modality is limited by the bandwidth for a fixed wavelength, we expected that the resolution of elastography would be limited by the bandwidth for a fixed wavelength. Therefore, we investigated the effect of a variation of the fractional bandwidth on the resolution for fixed ultrasonic frequencies as well. Previous work in the elastographic field suggested an empirical relationship between Z and bandwidth (Varghese and Ophir 1996). The shift between windows ΔZ could be considered as a fixed percentage of Z. Two other parameters that could influence the elastographic axial resolution are the beamwidth and the lesion/background elastic contrast. These two parameters cannot be directly related to the ultrasonic frequency. However, we could consider them constant for any given model.

The measurements shown in this paper were obtained using a particular mechanical model. Measuring the resolution as the smallest resolvable distance between two targets is a known model for resolution that conforms to the previous literature related to the resolution of an imaging modality (Callaghan 1991; Cook et al. 2000; Houston 1934; Rayleigh 1879; Schmitt et al. 1999). The method that we used to estimate the elastographic resolution from the strain images can be considered an extension of the Rayleigh criterion in the case of two inclusions with Gaussian elastic profile. The Rayleigh criterion, sometimes modified and/or extended, belongs to the category of two-target criteria that are widely used to define the resolution of a medical imaging modality (Callaghan 1991; Cook et al. 2000; Schmitt et al. 1999). Usually, however, the targets are point sources and the resolution is defined as the minimum distance between the two points. In elastography, the detectability of lesions depends on their size and contrast and on the strain noise in the elastograms (Belaid et al. 1994; Varghese and Ophir 1998). Therefore, the use of point sources for characterizing the resolution in elastography may not be appropriate, since elastography relies on interval estimation of strain rather than on point estimation. We believe that this assumption, together with the assumptions of a lossless medium and lack of additive noise dramatically influenced our measurements.

For this study, we initially considered the simplifi-

cation of no lateral and out-of-plane motions. Thereafter, we removed this simplification, estimated the axial resolution in the case of possible lateral motion of scatterers and compared the new measurements with the previous ones obtained under the assumption of no lateral motion. Statistical analysis showed that no statistically significant difference exists between the two sets of measurements. This may be explained by the fact that our measurements were obtained around the axis of symmetry of the target where the lateral and elevational motion is indeed minimized.

As previously mentioned, the stiffness distribution of the lesions was chosen to be Gaussian to reduce the strain concentrations around and between the lesions. It is known that abrupt discontinuities in the stiffness profile of a lesion under compression give rise to strain concentrations near the lesion (Kallel and Ophir 1998; Ophir et al. 1996). In the case of stiff cylindrical lesions, the strain concentrations resemble an upright cross (Kallel and Ophir 1998) which, in our case, would magnify the separation gap between the inclusions. Because we were interested in accurate measurements of the distance between the boundaries of the two lesions, in our model, we had to minimize the presence of these strain concentrations that could compromise a correct estimation of that distance. The use of a Gaussian distribution significantly reduces the presence of strain concentrations near the lesions (Kallel et al. 2001) and does not detract from the basic general result. Moreover, in practice, the condition of a discontinuous modulus change at the inclusion/background interface may not always be valid. For instance, in healthy tissues, the change in tissue structure may be gradual, which may also result in a gradual change of modulus distribution (Kallel et al. 1998, 2001).

A lesion/background elastic modulus contrast of 10:1 appeared to be appropriate for the purpose of this study. We also observed that the resolution does not change for a low contrast of 2:1, when compared to the higher contrast case of 10:1, provided that we averaged a sufficiently high number of independent realizations to reduce the noise. The need for more averaging is probably related to the fact that when the lesion/background elastic modulus contrast decreases, the CNRe decreases as well (Varghese and Ophir 1998), compromising the ability to precisely estimate the correct distance between lesions.

It should be noted that the resolution of any imaging system depends on the specifics of the target that is imaged and the model that is used for the estimation. In general, the values of the measured elastographic axial resolution may change if we adopt a different model and/or if any of the above assumptions would not hold. However, the functional form of the resolution should generally be independent of the target that was chosen, as shown for other imaging modalities (Foster et al. 2000; Wells 1977). Of course, the effect of the above assumptions on the measured resolution should be investigated in future work.

This paper has three important results. First, the axial resolution in elastography, as in sonography, is found to be proportional to the ultrasonic wavelength for a fixed fractional bandwidth, and is inversely proportional to the fractional bandwidth for a fixed ultrasonic wavelength (Figs. 5 and 9). Therefore, the empirical expressions of the axial resolution in elastography and in sonography are similar (both are proportional to λ and Q). However, the two constants of proportionality should be, theoretically, different because they have to take into consideration different parameters and/or the same parameters may influence the resolution differently. Moreover, the axial resolution in elastography is proportional to the wavelength, provided that all the other elastographic parameters are constant (*i.e.,* fractional bandwidth, beamwidth, and elastic contrast) or related to the wavelength as well (*i.e.,* cross-correlation window length, shift between consecutive windows). We have shown the effects of varying some of these parameters. The effect of the cross-correlation window length is not a linear one and, for a given frequency, there exists an optimal range of cross-correlation window lengths that gives the best resolution (Figs. 7, 8 and 13). This is somewhat contradictory to some of the previous literature. In fact, for many years, the resolution in elastography has been considered to be simply equivalent to the cross-correlation window length itself, with smaller Z producing improved resolution (Cespedes 1993; Varghese et al. 1998). This, however, seems to be true only until a certain value of Z is reached, below which the resolution apparently becomes limited by the wave parameters and no longer improves decreasing Z (Fig. 13). This result is, indeed, consistent with the results of Alam et al. (2000), who also showed that the window shift ΔZ has a significant effect on the effective elastographic resolution. They also found, in agreement with our results, that below a certain value of ΔZ (approximately 1% to 6% of Z), the resolution becomes insensitive to the value of ΔZ used to process the data. Based upon their results, we initially considered ΔZ as a small fixed percentage of Z (5%). Thereafter, we investigated the effect of a variation of ΔZ on the resolution as well (Fig. 15). From the results of Figs. 13 and 15, we can draw two important conclusions. First, the resolution can be compromised by an inappropriate choice of the cross-correlation window length Z and/or the window shift ΔZ. Second, an optimal range of values for Z (Fig. 13) and ΔZ (Fig. 15) exist that permit the best achievable elastographic axial resolution for a given US system.

Second, the cross-correlation window length Z that

gives the best resolution is proportional to the ultrasonic wavelength for a fixed fractional bandwidth and inversely proportional to the fractional bandwidth for a fixed ultrasonic wavelength (Figs. 6 and 10). From this conclusion, it appears that Z is a measure of resolution. However, it is important to observe that the optimal Z is not an independent parameter, but it is inversely proportional to the bandwith of the US system. In this context, the optimality of Z is related to the elastographic axial resolution although, previously an optimal Z was defined in relation to the SNRe (Varghese et al. 1998). The existence of an empirical relationship between Z and bandwidth has already been shown previously (Varghese and Ophir 1998). However, no systematic study has been done until now to accurately determine this relationship, which may be explained in the following way: It is known that the SNRe depends on the bandwidth and/or the center frequency and the cross-correlation window length (Varghese and Ophir 1997). Therefore, a bandwidth and/or a center frequency increase (decrease) would lead to a corresponding decrease (increase) of the window length to maintain the same precision of the time-delay estimation, and, ultimately, the same SNRe. This is qualitatively confirmed by the fact that the axial resolution and the optimal Z show a "similar" dependence on the wavelength (*i.e.,* similar constants of proportionality) (Figs. 5 and 6).

Third, the axial resolution in elastography is on the same order of magnitude as the axial resolution in sonography. A simplified theoretical expression for the sonographic axial resolution for a spherical radiator at the focus is given by eqn (1) (Christensen 1988). It has also been reported that, in general, a typical US system has range resolutions (*i.e.,* resolution along the axis) corresponding to 1.2, 2.5 and 3.0 wavelengths, at dynamic ranges of 10, 20 and 30 dB, respectively (Wells 1977). Although the resolution of a US system may be defined in a number of different ways (Wells 1977), it has been well known that the sonographic axial resolution is on the order of the wavelength (Christensen 1988; Foster et al. 2000; Wells 1977). The present study shows that the elastographic axial resolution is on the order of the wavelength as well (Figs. 5 and 9) and, therefore, it is on the same order of magnitude as the ultrasonic resolution. As expected, the measured values of the elastographic axial resolution reported in Figs. 5 and 9 are larger than those obtained for sonography simply by applying the theoretical formula, eqn (1). This may be due to several factors. First of all, the theoretical formula refers to a bandwidth at -3-dB. For a bandwidth defined as the frequency width of the power spectral density at -6-dB, which is what we used in this study, the theoretical formula must be derated (*i.e.,* the resolution is worse) by a factor of $\sqrt{2}$. Moreover, the theoretical formula does not take into consideration the numerous factors that, in practice, would limit the measured resolution, such as the limitations imposed by noise and the distance from the transducer (Wells 1977). On the contrary, in our study, we have simulated a real experimental situation, with a real US system, and we have used a conservative method to estimate the elastographic resolution. However, even considering some of these factors that may, in practice, corrupt the sonographic values given by the theoretical formula, we may still expect the measurements of the axial resolution in elastography to be slightly larger than those obtained for sonography. This may be due to several reasons. The presence of noise, introduced by the gradient operation together with stretching, necessitates filtering the data to improve the accuracy of the measurements. We applied a median filter with a subwavelength kernel size. Because it was found that the elastographic resolution is on the order of the wavelength, it is expected that such a filter would not significantly deteriorate the actual resolution. However, in general, any low-pass filtering operation tends to smooth the images, therefore increasing the SNR but, also, compromising the spatial resolution. This may also explain the slight overestimation of the elastographic axial resolution when compared to the known real distance obtained from the modulus image (compare the real values shown at the bottom of Fig. 4 with the data points plotted in Fig. 5). Observe also that the strain estimation method used for these measurements performs a global temporal stretching of the postcompression A-line before the cross-correlation analysis (Varghese and Ophir 1997). Temporal stretching reduces axial signal decorrelation, which has a significant impact on the SNRe, sensitivity and dynamic range (Varghese and Ophir 1996). Although this operation is necessary to perform the measurements, especially for high frequencies, it will generally not be correct for all strains in the elastograms. In fact, the distribution of the strain in the elastograms is nonuniform, due to the presence of regions of different stiffness. Therefore, a global uniform stretching will improve the SNRe only for certain portions of the tissue. An adaptive stretching method used in conjunction with the gradient method could improve the obtainable resolution (Alam et al. 1998). Also, the mechanical strain concentrations around the lesions, although reduced by the use of Gaussian models, may not be completely eliminated (see Fig. 4) and may compromise the estimation of the real distance between lesions.

CONCLUSIONS

We have shown that the attainable axial resolution in elastography is directly proportional to the wavelength, and inversely proportional to the bandwidth of

the US system used to acquire the data. Therefore, the axial resolution in elastography is ultimately limited by the ultrasonic pulse width, or, equivalently, by the bandwidth of the US system. The DSP parameters used to process the data were found to influence the attainable resolution. An inappropriate choice of these parameters may seriously degrade the resolution. An optimal cross-correlation window length exists that is proportional to the pulse width of the system as well. The results suggest that, like sonography, elastography may be scaled up to high frequencies with a corresponding increase in resolution. Therefore, elastography may have significant potential for applications where the use of high frequency is required to obtain acceptable resolution.

REFERENCES

Alam K, Ophir J, Konofagou EE. An adaptive strain estimator for elastography. IEEE Trans Ultrason Ferroelect Freq Contr 1998;45: 461–472.

Alam K, Ophir J, Varghese T. Elastographic axial resolution: An experimental study. IEEE Trans Ultrason Ferroelect Freq Contr 2000;47:304–309.

Belaid N, Cespedes EI, Thijssen JM, Ophir J. Lesion detection in simulated elastographic and echographic images: A psychophysical study. Ultrasound Med Biol 1994;20:877–891.

Callaghan PT. Principles of nuclear magnetic resonance microscopy. Oxford: Claredon Press, 1991.

Cespedes EI. Elastography. Imaging of biological tissue elasticity. Ph.D. Dissertation, University of Houston, Houston, TX, 1993.

Christensen C. Ultrasonic bioinstrumentation. New York: John Wiley & Sons, 1988.

Cohn AN, Emelianov SY, O'Donnel M. An elasticity microscope. Part I: Methods. IEEE Trans Ultrason Ferroelect Freq Contr 1997;44(6): 1304–1319.

Cook LT, Zhu Y, Hall TJ, Insana MF. Bioelasticity imaging II. Spatial resolution. Proceedings of the SPIE Medical Imaging 2000: Ultrasonic imaging and signal processing. 2000;3982:315–324.

Fortin M, Buschmann MD, Bertrand MJ, Foster FS, Ophir J. Cross-correlation of ultrasound A-lines to obtain dynamic displacement profiles within poroelastic materials undergoing stress relaxation. Proceedings of the SPIE The International Society for Optical Engineering. 2000;3982:286–294.

Foster FS, Pavlin CJ, Harasiewicz KA, Turnbull DAC, Turnbull DH. Advances in ultrasound biomicroscopy. Ultrasound Med Biol 2000; 26:1–28.

Gaskill JD. Linear systems, Fourier transforms, and optics. New York: John Wiley & Sons, 1978.

Houston WV. Principles of mathematical physics. New York: McGraw-Hill, 1934.

Kallel F, Ophir J. Limits on the contrast of strain concentrations in elastography. Ultrasound Med Biol 1998;24:1215–1219.

Kallel F, Ophir J, Magee K, Krouskop TA. Elastographic imaging of low-contrast elastic modulus distributions in tissue. Ultrasound Med Biol 1998;24:409–425.

Kallel F, Prihoda CD, Ophir J. Contrast-transfer efficiency for continuously varying tissue moduli: Simulation and phantom validation. Ultrasound Med Biol 2001;8:1115–1125.

Konofagou EE, Ophir J, Kallel F, Varghese T. Elastographic dynamic range expansion using variable applied strains. Ultrason Imaging 1997;19:145–166.

Ophir J, Alam K, Garra B, Kallel F, Konofagou EE, Krouskop TA, Varghese T. Elastography: Ultrasonic estimation and imaging of the elastic properties of tissues. Proceedings of the Institution of Mechanical Engineers, Part H. J Eng Med 1999:1–31.

Ophir J, Cespedes EI, Garra B, Ponnekanti H, Huang Y, Maklad N. Elastography: Ultrasonic imaging of tissue strain and elastic modulus in vivo. Eur J Ultrasound 1996;3:49–70.

Ophir J, Cespedes EI, Ponnekanti H, Yazdi Y, Li X. Elastography: A quantitative method for imaging the elasticity of biological tissues. Ultrason Imaging 1991;13:111–134.

Ponnekanti H, Ophir J, Huang Y, Cespedes EI. Fundamental mechanical limitations on the visualization of elasticity contrast in elastography. Ultrasound Med Biol 1995;21:533–543.

Rayleigh S. Acoustical observations. Phil Mag 1879;261–274.

Righetti R. Axial resolution in elastography. MA Thesis, University of Houston, TX, 2001.

Schmitt JM, Bao X, Xiao S. Micro-elastography of tissue with OCT. Proceedings-SPIE The International Society for Optical Engineering. 1999;3598:47–55.

Varghese T, Ophir J. Performance optimization in elastography: Multicompression with temporal stretching. Ultrason Imaging 1996;18: 193–214.

Varghese T, Ophir J. Enhancement of echo-signal correlation in elastography using temporal stretching. IEEE Trans Ultrason Ferroelec Freq Contr 1997;44(1):173–180.

Varghese T, Ophir J. An analysis of the elastographic contrast-to-noise ratio performance. Ultrasound Med Biol 1998;24:915–924.

Varghese T, Bilgen M, Ophir J. Multiresolution imaging in elastography. IEEE Trans Ultrason Ferroelect Freq Contr 1998;45(1):65–75.

Wells PNT. Biomedical ultrasonics. New York: Academic Press, 1977.